Shear attenuation and anelastic mechanisms in the central Pacific upper mantle

Zhitu Ma[1,2], Colleen A. Dalton[2], Joshua B. Russell[3], James B. Gaherty[3,4], Greg Hirth[2], Donald W. Forsyth[2]
1. State Key Laboratory of Marine Geology, Tongji University 2. Department of Earth, Environmental and Planetary Sciences, Brown University
3. Lamont-Doherty Earth Observatory, Columbia University 4. School of Earth and Sustainability, Northern Arizona University

EGU General Assembly 2020
EGU 2020 Share Geoscience Online
Contact zhitu_ma@tongji.edu.cn

A. Abstract and summary of result

We determine the mantle attenuation (1/Qμ) structure beneath 70 Myr seafloor in the central Pacific by the NoMelt array. After the removal of tilt and compliance noise, we are able to measure Rayleigh wave phase and amplitude for 125 earthquakes. Attenuation and azimuthally anisotropic phase velocity in the study area are determined by approximating the wavefield as the interference of two plane waves. We find that the amplitude decay of Rayleigh waves across the NoMelt array can be adequately explained using a two-layer model: Qμ=1400 in the shallow layer, Qμ=110 in the deeper layer, and a transition depth at 70 km, although the sharpness of the transition is not well resolved.

Notably, Qμ observed in the NoMelt lithosphere is significantly higher than values in this area from global attenuation models. When compared with lithospheric Qμ measured at higher frequency (~3 Hz), the frequency dependence of attenuation is very slight.

We also use laboratory-based parameters to predict attenuation and velocity-dispersion spectra that result from the superposition of a weakly frequency dependent high-temperature background and an absorption peak. We test a large range of frequencies for the position of the absorption peak (fe) and determine, at each depth, which values of fe predict the observed Qμ and Vs simultaneously. We show that between depths of 60 and 80 km, the seismic models require an increase in fe by at least 3-4 orders of magnitude. Under the assumption that the absorption peak is caused by elastically accommodated grain-boundary sliding, this increase in fe reflects a decrease in grain-boundary viscosity of 3-4 orders of magnitude. A likely explanation is an increase in the water content of the mantle, with the base of the dehydrated lid located at ~70-km depth.

B. Data and noise removal

We examine all the earthquakes with magnitudes greater than 5.5 in the GCMT catalog (Ekström et al. 2012; Dziewonski et al. 1981) in 2012. We follow closely the procedure described in Bell et al. (2014) to remove compliance and tilt noise on the vertical component of the OBS data.

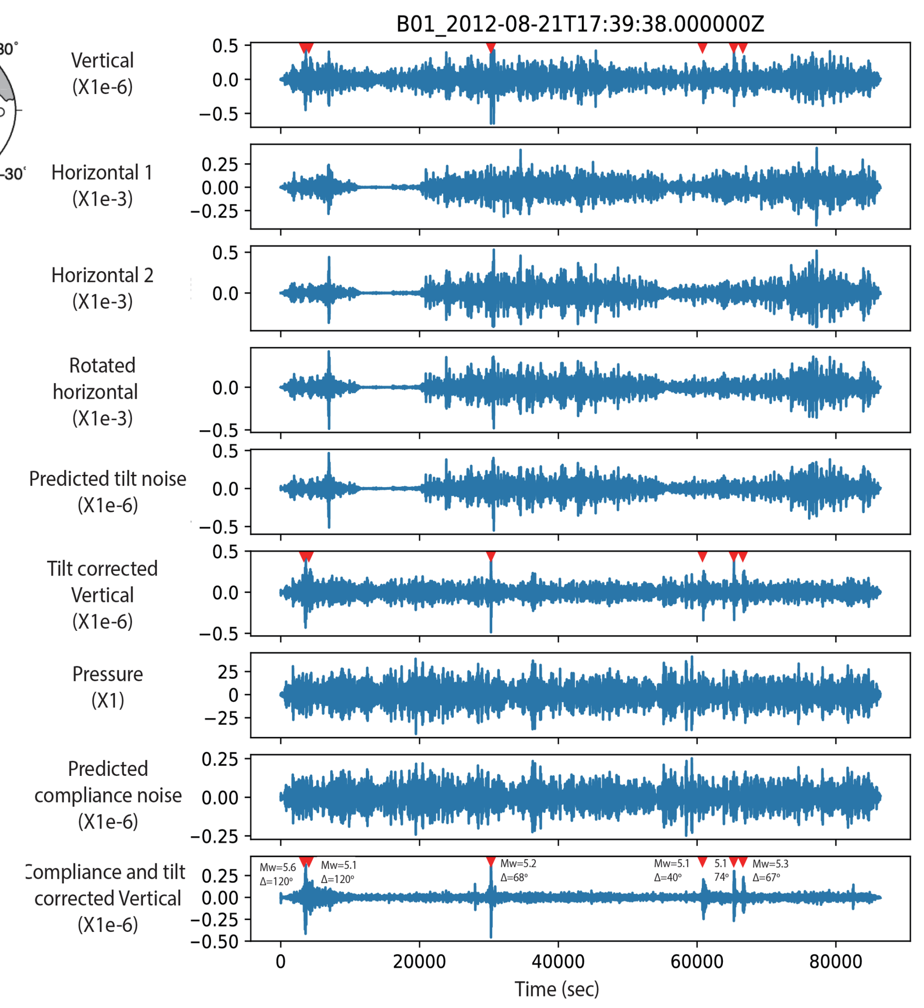

Figure 1: Top: Earthquakes used in this study (white circles) and the location of NoMelt array (yellow triangles). Right: Example of waveforms showing the effect of removing tilt and compliance noise. All waveforms have been bandpass filtered between 10 and 50 mHz. Removing tilt and compliance noise clearly make the earthquakes (Mw>5 in the GCMT catalog) more visible.

C. Averaged phase velocity and amplitude decay

Example of the recorded waveforms and amplitudes

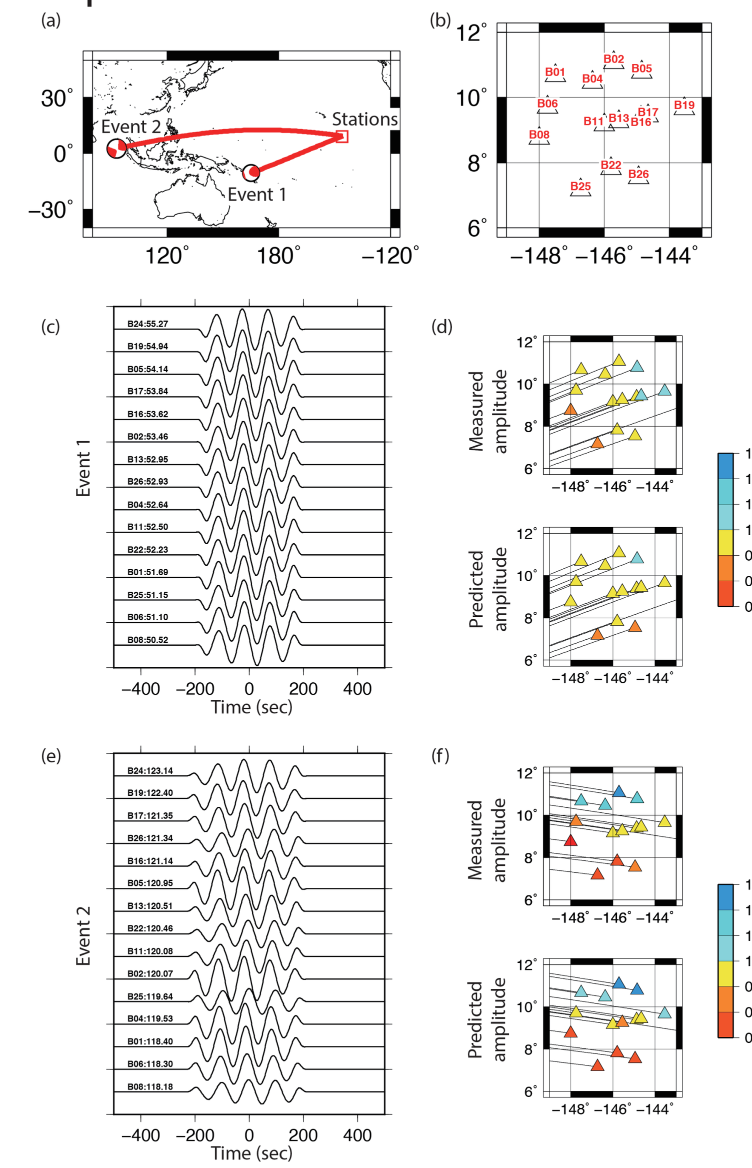

Figure 2 (a) Locations for two example events. (b) Stations used in this study. (c) Waveforms for event 1 bandpass filtered at 10 mHz. (d) The measured and predicted amplitudes. (e-f) same as (c-d), but for event 2.

While event 1 produces almost identical traces, the waveforms from event 2 are clearly affected by off-great-circle wave interference (Forsyth and Li, 2005). However, in both cases, the amplitudes can be well reproduced by the two-plane wave method.

The averaged phase velocity and amplitude dacay

At each frequency, we incorporate all events simultaneously to solve for 2D phase velocity variation, 1D average azimuthal anisotropy and 1D average amplitude decay coefficient within the region.

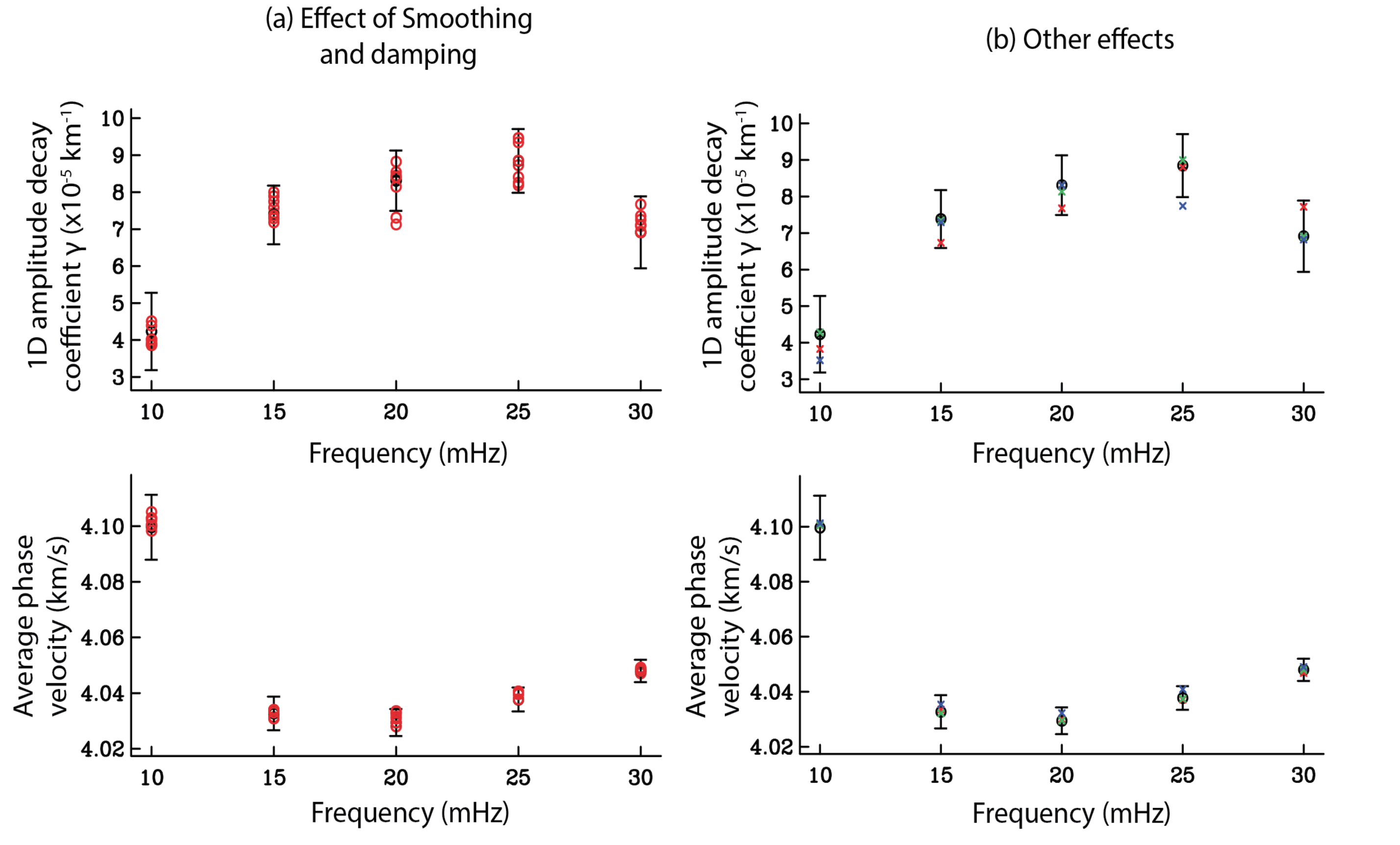

Figure 3: The averaged phase velocity and amplitude decay (black error bars). The effect of smoothing and damping (red circles, left), the inversion region (blue crosses, right), the starting value of γ (green crosses, right), whether or not including a station term (red crosses, right) is small.

D. 1D shear wave velocity and attenuation at depth

The inversions are based on linearized perturbation theory (Dziewonski and Anderson 1980; Woodhouse 1980) where the sensitivity kernels K are shown in Fig 4:

$$\delta c(\omega) = \int_0^a K_{SV}(\omega,r)\,\delta V_{SV}(r)\,dr$$

$$Q^{-1}(\omega) = \int_0^a K_{Q\mu}(\omega,r)\,Q_\mu^{-1}(r)\,dr$$

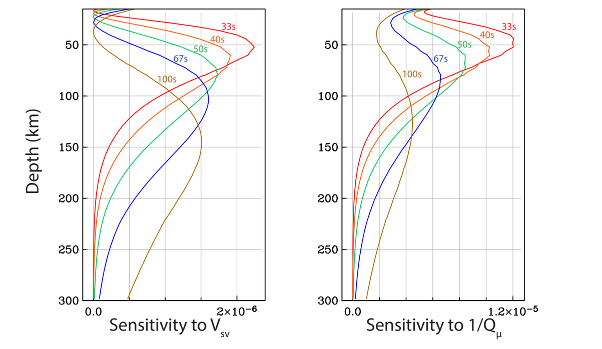

Figure 4: Sensitivity kernels of Rayleigh wave phase velocity and attenuation to V_{sv} and $1/Q_\mu$.

Shear wave velocity

In the inversion, we test two reference models: , one that is smooth in the mantle (S) and one that contains a 5% velocity reduction from 60 km to 65 km in depth (D, Mark et al. 2019). For radial anisotropy, we assume it is either ~3% (SH, Nishimura and Forsyth, 1989; Gaherty et al., 1996) or the value in SEMum2 (SH-2, French et al., 2013). We combine our data with the ones in Lin et al. (2016) and Russell et al. (2019) in the final inversion.

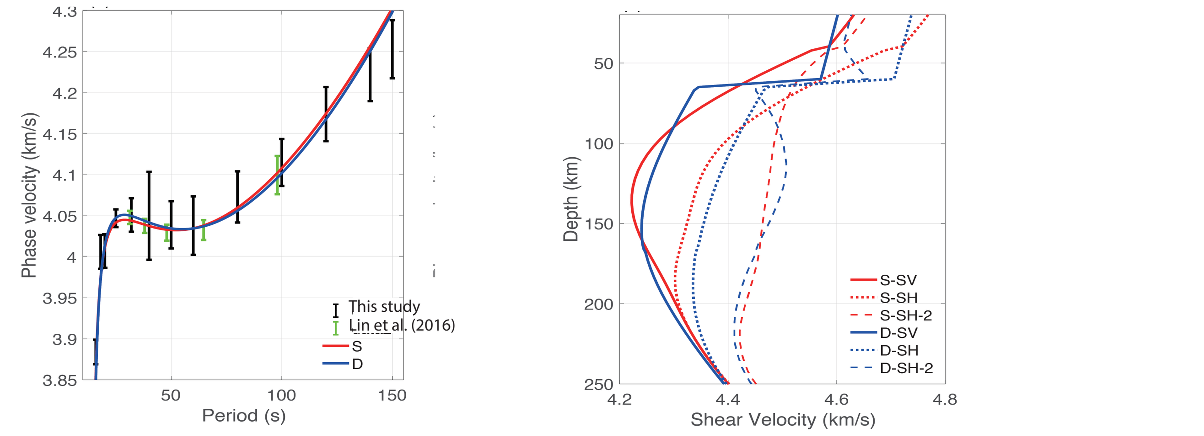

Figure 5: (Left) Measured and predicted fundamental-mode Rayleigh wave phase velocity from the inversed model. (Right) Vertically (SV) and horizontally (SH) polarized shear velocity for the smooth (S) and discontinuous (D) final velocity models.

Shear attenuation

We first perform a grid search and find that a model with only two layers of Q_μ is sufficient to explain our data (Fig. 6 and 7). We then perform a non-negative-least-square inversion (Lawson and Hanson 1995) using this two layer model as the starting model (Fig. 7).

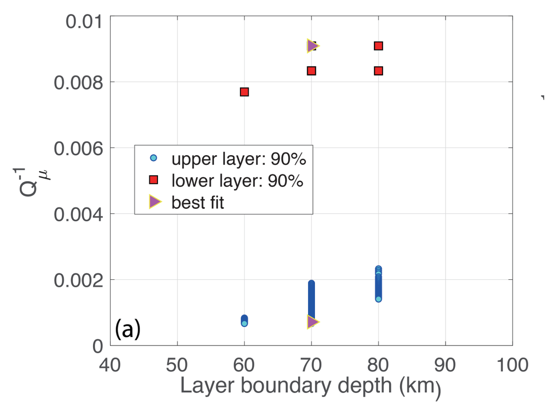

Figure 6: Results of grid search for two-layer model. We test Qμ from 50 to 1500 in increments of 10 and depth of the layer boundary from 0 to 400 km in increments of 10 km. Symbols show acceptable models (90% confidence level) and the lowest-misfit model.

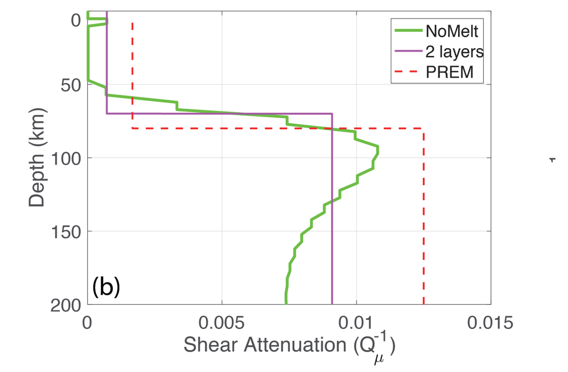

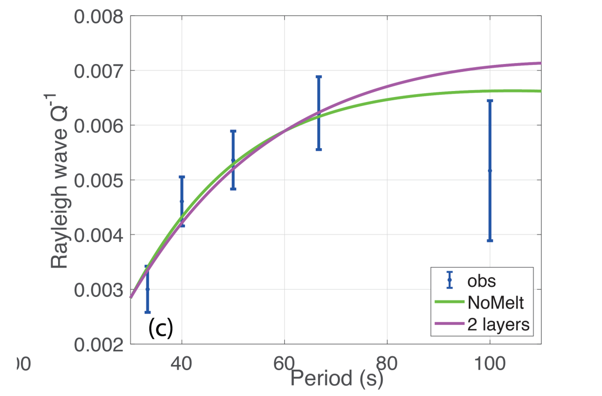

Figure 7: (Top) Depth profiles of shear attenuation for the two-layer and final models, compared to PREM. (Bottom) Observed and predicted Rayleigh wave attenuation.

E. Discussion

Comparison with attenuation at higher frequency

The difference in the frequency dependence of Q_μ between lithosphere and asthenosphere is smaller than what was suggested by Takeuchi et al. (2017) (Fig. 8).

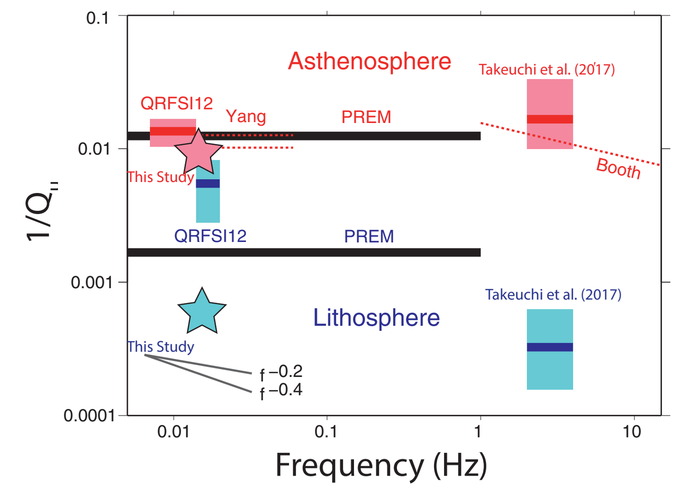

Figure 8: Comparison between the attenuation in this study (star), QRFSI12 (Dalton et al. 2008), Yang and Forsyth (2007), PREM (Dziewonski and Anderson 1981), Takeuchi et al. (2017) and Booth et al. (2014). This figure is modified from Takeuchi et al. (2017).

Comparison with laboratory measurement

We first compute the anharmonic correction of anelasticity on shear wave speed (Vs/Vs^{anh}) by comparing our inverted values with the ones obtained from Perple_x.

We then model the deformation mechanism by supersition of two spectra: the high temperature background (HTB) and the elastically accommodated grain-boundary sliding (EAGBS) according to the shape given in Jackson and Faul (2010) but modify the peak frequency fe of the EAGBS.

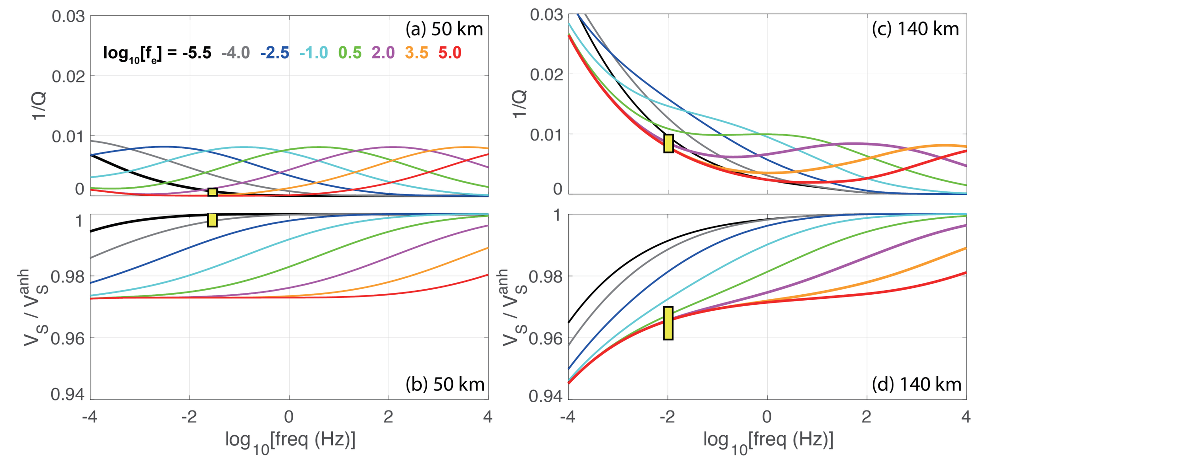

Figure 9. Predicted and measured spectra of attenuation and shear-velocity reduction at 50 and 140 km. We grid search for the best-fitting fe. The small yellow boxes enclose the range of NoMelt values.

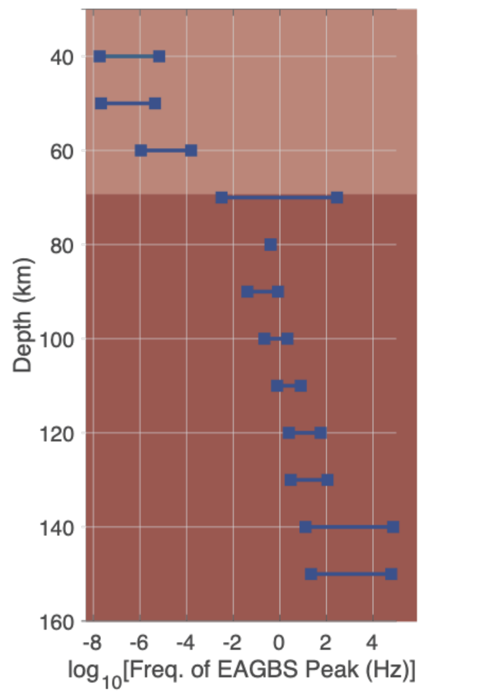

Figure 10. Ranges of fe that can predict the observed shear wave speed and attenuation in this study simultaneously. Notice the sharp change at ~70 km. We assume that the attenuation peak is due to EAGBS and fe is related to grain boudary viscosity, thickness, grain size and unrelaxed shear modulus. The most likely change at this magnitude is likely caused by a change in viscosity, which indicates a possible change of water content at this depth.